ISPRS Journal of Photogrammetry and Remote Sensing 141 (2018) 265–274

Contents lists available at ScienceDirect

ISPRS Journal of Photogrammetry and Remote Sensing

journal homepage: www.elsevier.com/locate/isprsjprs

Adaptive stopping criterion for top-down segmentation of ALS point clouds in temperate coniferous forests

Nina Amiri[a,b,*], Przemyslaw Polewski[c], Marco Heurich[d], Peter Krzystek[a], Andrew K. Skidmore[b,e]

[a] Department of Geoinformatics, Munich University of Applied Sciences, 80333 Munich, Germany
[b] Faculty of Geo-Information Science and Earth Observation, University of Twente, P.O. Box 217, 7500 AE Enschede, The Netherlands
[c] MUVI Smart Tech GmbH, Marcel-Breuer-Str. 15, 80807 Munich, Germany
[d] Chair of Wildlife Ecology and Management, University of Freiburg, Freiburg, Germany
[e] Department of Environmental Science, Macquarie University, NSW 2106, Australia

ARTICLE INFO

Keywords:
ALS 3D point clouds
Single tree segmentation
Quadratic surfaces
Elliptic paraboloid fitting

ABSTRACT

The development of new approaches to individual tree crown delineation for forest inventory and management is an important area of ongoing research. The increasing availability of high density ALS (Airborne Laser Scanning) point clouds offers the opportunity to segment the individual tree crowns and deduce their geometric properties with a high level of accuracy. Top-down segmentation methods such as normalized cut are established approaches for delineation of single trees in ALS point clouds. However, overlapping crowns and branches of nearby trees frequently cause over- and under-segmentation due to the difficulty of defining a single criterion for stopping the partitioning process. In this work, we investigate an adaptive stopping criterion based on the visual appearance of trees within the point clouds. We focus on coniferous trees due to their well-defined crown shapes in comparison to deciduous trees. This approach is based on modeling the coniferous tree crowns with elliptic paraboloids to infer whether a given 3D scene contains exactly one or more than one tree. For each processed scene, candidate tree peaks are generated from local maxima found within the point cloud. Next, paraboloids are fitted at the peaks using a random sample consensus procedure and classified based on their geometric properties. The decision to stop or continue partitioning is determined by finding a set of non-overlapping paraboloids. Experiments were performed on three plots from the Bavarian Forest National Park in Germany. Based on validation data from the field inventory, results show that our approach improves the segmentation quality by up to 10% across plots with different properties, such as average tree height and density. This indicates that the new adaptive stopping criterion for normalized cut segmentation is capable of delineating tree crowns more accurately than a static stopping criterion based on a constant Ncut threshold value.

1. Introduction

Accurate measurements of forest resources are essential for precise and sustainable forest management (Chang et al., 2013). Single tree attributes, such as tree crown base height, volume, DBH (Diameter at Breast Height), position, height, and species, are required for quantitative forest analysis and ecosystem management services (Hu et al., 2014; Yao et al., 2012). Currently, most of those variables are estimated by measuring a set of sample plots manually in field surveys, thus, forest inventories are expensive and time consuming. Recently, many studies have been focused on decreasing costs by developing inventory methods that are based on remote sensing techniques.

Airborne Laser Scanning (ALS) has become a key tool for gathering information on 3D structures in forests (Wulder et al., 2012). Information derived from ALS data can provide detailed forest characteristics and serve as a basis for single tree analysis (Wagner et al., 2008; Reitberger et al., 2009). The information extracted from segmented trees, e.g. tree height or crown diameter, is often used as the independent variable in allometric modeling of additional individual tree characteristics such as stem volume, leaf area index, and biomass, as well as entire forest stands (Yao et al., 2012; Yu et al., 2011). Therefore, any inaccuracy in tree delineation, which is often caused by over- or under-segmentation, will transfer to these characteristics.

Several methods for detecting and delineating single tree crowns using ALS point clouds have been proposed in the literature, based on two main types of data: the ALS-derived Canopy Height Model (CHM)

* Corresponding author at: Department of Geoinformatics, Munich University of Applied Sciences, 80333 Munich, Germany.
E-mail addresses: n.amiri@hm.edu, n.amiri@utwente.nl (N. Amiri), przemyslaw.polewski@muvi-smart-tech.com (P. Polewski), marco.heurich@wildlife.uni-freiburg.de (M. Heurich), krzystek@hm.edu (P. Krzystek), a.k.skidmore@utwente.nl, andrew.skidmore@mq.edu.au (A.K. Skidmore).

https://doi.org/10.1016/j.isprsjprs.2018.05.006
Received 14 November 2017; Received in revised form 9 March 2018; Accepted 11 May 2018
Available online 29 May 2018

and the original ALS point cloud. In the first method, tree crowns are found using the watershed algorithm (Pyysalo and Hyyppä, 2002) or a slope-based segmentation (Hyyppä et al., 2001; Persson et al., 2002). The study of Persson et al. (2002) indicates a detection rate of 71% for a boreal forest dominated by spruce and pine trees. Later, Solberg et al. (2006) proposed a region growing method that starts from local surface maxima and finds crown polygons. The method was applied to a structurally heterogeneous spruce forest with an overall detection rate of 66% for the CHM, which was smoothed with a Gaussian filter. Heurich (2008) demonstrated that the segmentation method of Persson et al. (2002) leads to an average detection rate of 45% in the Bavarian Forest National Park. The segmentation results of the studies mentioned above illustrate the strong dependency on forest type.

In contrast, point cloud-based methods take advantage of the captured 3D information and focus on the detection of single tree objects, which are the tree as a whole or parts of the tree, such as stems and branches (Wu et al., 2016; Zhang et al., 2003). Several approaches have been developed for extracting single trees from ALS 3D point clouds. Morsdorf et al. (2004) used the *k*-means clustering algorithm to segment single trees from raw ALS point clouds. However, the accuracy of their study is highly dependent on seed points extracted from the CHM. Wang et al. (2008) subdivided the forest into different layers and applied a 2D morphological algorithm to obtain tree crowns. Reitberger et al. (2009) introduced a novel normalized cut segmentation method that extracts single trees using a graph cut approach. The study successfully showed that the overall accuracy of extraction of individual tree crowns in heterogeneous forest types could be significantly improved (by up to 20%), especially in the lower forest layers. Lee et al. (2010) proposed an adaptive region growing and clustering approach to detect single trees directly within raw point clouds. Li et al. (2012) developed a spacing-based algorithm that utilizes a region growing approach to segment trees in a coniferous mixed forest. Véga et al. (2014) suggested the PTrees method to extract trees in a forest from ALS data. The method is a multi-scale dynamic segmentation at point cloud level. Wu et al. (2016) developed an automated segmentation method that captures the topological structure of forests and assesses the topological relationships of tree crowns by using a graph theory-based localized contour tree method, achieving an overall accuracy of up to 94%.

The forest structure has a strong impact on the single tree segmentation performance. Tree crowns have a complex shape that varies significantly from species to species. The accuracy of single tree delineation algorithms mainly depends on the complexity of the forest (Strîmbu and Strîmbu, 2015; González-Ferreiro et al., 2013; Vauhkonen et al., 2011). Moreover, segmentation algorithms are controlled by many parameters that are difficult to estimate when the methods are applied to other forest types. This dependency can be either explicit, as with the number of seed points in k-means, or implicit, such as the *Ncut* threshold for spectral clustering methods. The incorrect setting of such parameters may lead to over- or under-segmentation effects in the resulting delineated trees (Strîmbu and Strîmbu, 2015; Khosravipour et al., 2014; Yao et al., 2014; Li et al., 2012; Heurich, 2008). Although the control parameters can be estimated by a grid search method for a localized forest area, their transferability to larger scenes can be poor. Therefore, if the fixed scheme of control parameters in the segmentation algorithm is replaced by an adaptive scenario applied on the decision level, a more flexible tree crown delineation procedure is to be expected.

The main objective of this study is to develop a new adaptive stopping criterion, applicable to top-down segmentation methods for precise delineation of single trees in ALS 3D point clouds. Their parameters can be automatically determined from reference segmentations, alleviating the burden of manual, trial-and-error parameter setting. Moreover, the adaptive procedure is based solely on the appearance of the target objects (tree crowns) within the point cloud, and is independent of any internal features of the underlying segmentation method. For the time being, we restrict our attention to coniferous trees whose well-defined crown shape can be easily modeled by an elliptic paraboloid (Koop, 1989; Husch et al., 2002). This study is motivated by the successful application of an adaptive stopping criterion to the segmentation of lying dead trees based on the normalized cut algorithm (Polewski et al., 2015). Here, we extend the idea of an appearance-based adaptive stopping criterion to the domain of single tree segmentation. We conducted a series of experiments on sample plots from the Bavarian Forest National Park to assess the performance of the proposed method using data from the field inventory for validation. In our experiments, the normalized cut algorithm was used as the segmentation method, but any other top-down clustering procedure could be applied instead.

The remainder of this work is structured as follows: Sections 2 and 3 describe the details of our approach; Section 4 illustrates the study area, materials, and field measurements. The results are presented and discussed in Section 5. Finally, the conclusions are stated in Section 6.

2. Top-down segmentation

2.1. Main foundation

The segmentation of point clouds into individual objects in the scene is an initial step in processing 3D point clouds. The main objective of the segmentation processes is to divide points with similar attributes into homogeneous clusters. Among the various approaches, a popular paradigm is *top-down* segmentation, where all objects are initially assigned to a single cluster, which is then recursively partitioned. The subdivision continues until the predefined stopping criterion is met. However, the main difficulty of these methods is the definition of an appropriate stopping criterion that yields meaningful clusters under varying input scenarios.

2.2. Normalized cut segmentation

The normalized cut algorithm (Shi and Malik, 2000) is a top-down method for data segmentation. This method to construct a low-dimensional representation of the input 3D points uses the eigenvalues associated with the object similarity matrix (Polewski et al., 2015). A graph is constructed based on the similarity matrix that quantifies pairwise compatibility between primitives from a predefined set, such as cubic voxels or irregular super-voxels provided by any kind of pre-segmentation like mean shift of *k*-means. A recursive bisection of the graph's vertices into disjoint clusters A and B is performed such that the within-cluster similarity is maximized while simultaneously the inter-cluster similarity is minimized. The corresponding normalized cut is:

$$NCut(A,B) = \frac{Cut(A,B)}{Assoc(A,V)} + \frac{Cut(A,B)}{Assoc(B,V)} \quad (1)$$

with $Cut(A,B) = \sum_{i\in A, j\in B} w_{ij}$ as the total sum of the weights between the segments A and B, while $Assoc(A,V) = \sum_{i\in A, j\in V} w_{ij}$ is the sum of weights of all the edges ending in segment A. The similarity function for the normalized cut is based on the pair-wise similarity of the clusters. The aforementioned segmentation is controlled by several parameters whose values can be optimized in experiments. The most important parameter that controls the subdivision of the graph is the normalized cut threshold, $NCut_{thr}$, which has no physical interpretation. During the segmentation, if the NCut value of the obtained clusters A and B exceeds $NCut_{thr}$ then the similarity between A and B is too high and the process must be terminated. Clearly, choosing a suitable threshold is critical to obtaining a reasonable segmentation, because too small a value of $NCut_{thr}$ will lead to under-segmentation with clusters consisting of unrelated objects. Conversely, too large a value will result in over-segmentation and many small clusters. In real world applications, setting the most suitable value for this static threshold is challenging

due to different input characteristics.

2.3. Other top-down algorithms

Although normalized cut is the most commonly-used of the top-down segmentation algorithms, other methods have also found use in various clustering applications. Two methods from the graph-cut family are “Min Cuts” (Wu and Leahy, 1993) as well as “MinMax Cut” (Nie et al., 2010), where the graph is partitioned according to different optimization objectives. Also, a recursive, bisecting version of k-means has been developed (Savaresi and Boley, 2001). Essentially, any of these mentioned algorithms could benefit from the proposed adaptive stopping criterion approach. In this work we decided to utilize the normalized cut procedure as the core method, because (i) the implementation could potentially be modified to optimize one of the other related criteria from the spectral clustering family (Min Cuts, MinMax Cut) with moderate effort, and (ii) the normalized cut has already been applied in literature for the problem of tree segmentation.

3. Adaptive stopping criterion

3.1. Outline

Consider a point cloud representing a forest scene with multiple coniferous trees. The normalized cut algorithm recursively partitions the 3D data, starting with the entire point cloud, until the level of single trees is reached. Let S_i represent an intermediate point cluster obtained at a recursion level m of the partitioning. S_i may contain one or more trees. The rationale of our adaptive stopping criterion is to detect tree crowns by fitting local quadratic surfaces to candidate tree tops, and using this information to determine whether the currently processed cluster of points represents a single or multiple trees. In the former case, the segmentation is stopped, otherwise the current cluster is split and the partitioning process continues. The method proceeds as follows. We use a local maxima detection approach to find candidate peaks of single trees. Then, we apply the Random Sample Consensus (RANSAC) method to estimate the best fitting quadratic surface parameters for points around each detected local maximum. The signed distances between the fitted surface and local points are binned to form histogram features. These features provide a basis for classifying the neighborhood of each local maximum, either as a true tree top or a false positive. After classification in a probabilistic manner, the spatial overlap ratios op_r (proportion of shared volumes) between all pairs of positively classified candidate tree tops are calculated. If a pair of fitted surfaces have an overlap ratio below a threshold value max_{op_r}, then it is decided that the current cluster contains more than one tree and the segmentation has to continue. If no such pair is found, the stopping criterion is activated and the segmentation of the current cluster is terminated. The entire processing pipeline is presented in Fig. 1. The method is explained in detail in the following sub-sections.

3.2. Local maxima detection

The input ALS data is a set of 3D point clouds with 3D coordinates $p_i(x_i,y_i,z_i)$ for each point. In our approach, the local maxima are detected only within a currently segmented scene in the normalized cut segmentation process. We examine a spherical neighborhood around each point to determine whether it has the locally maximal z coordinate. The neighborhood radius is balanced between permitting adjacent tree tops and not producing too many insignificant local maxima. Note that we do not apply a smoothing step to the original point clouds. Fig. 2 shows the detected local maxima for two clusters S_i and S_j with true tree tops and a false positive, respectively.

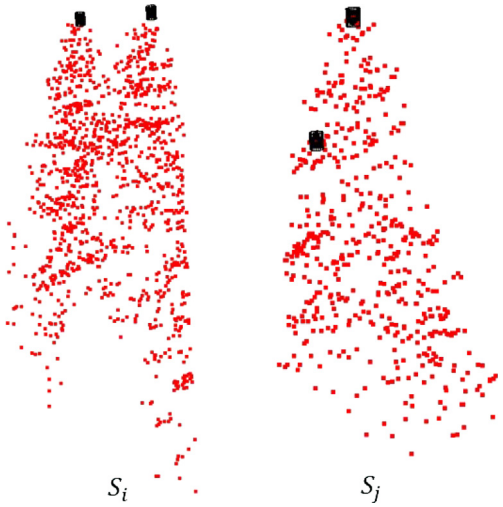

Fig. 2. Detected local maxima for two pairs of clusters S_i;S_j. S_i represents a cluster with 2 true tree tops; S_j shows a false positive scenario in the cluster, with at least one falsely detected local maximum.

3.3. Shape fitting with RANSAC

The Random Sample Consensus algorithm (Fischler and Bolles, 1981) is a general robust parameter estimation approach designed to deal with a large proportion of outliers in the input data. In this step, the algorithm is applied to estimate the best-fitting elliptic paraboloid parameters around each local maximum based on points inside a cylinder with a predefined length cyl_l and radius cyl_r. The parameters of the cylinder are defined experimentally. The center of the paraboloid is indicated by the inferred local maximum, and RANSAC is used to compute the remaining paraboloid parameters. Fig. 3 illustrates the fitted elliptic paraboloids based on detected local maxima for two clusters S_i and S_j.

3.3.1. Elliptic paraboloids

A second order algebraic surface is given by the following general equation

$$ax^2 + by^2 + cz^2 + 2fyz + 2gzx + 2hxy + 2px + 2qy + 2rz + d = 0 \quad (2)$$

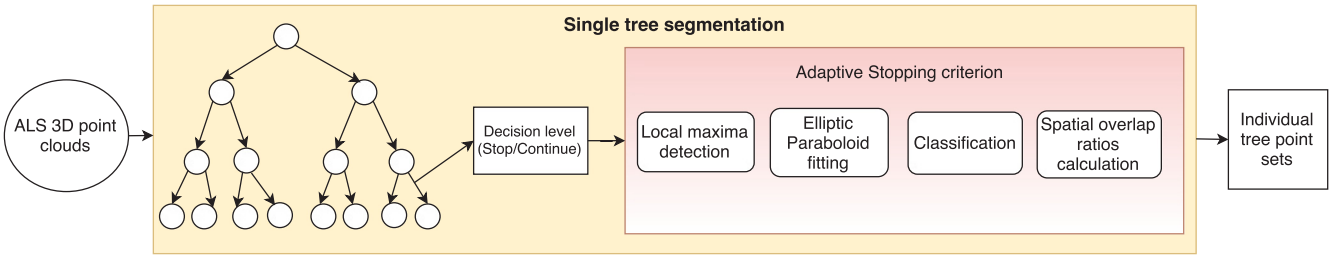

Fig. 1. Overview of single tree segmentation strategy using adaptive stopping criterion.

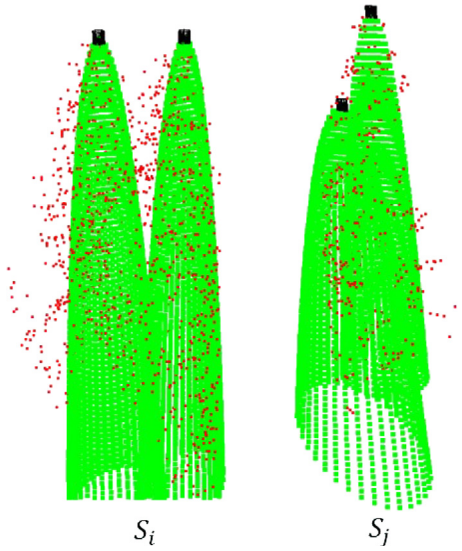

Fig. 3. Fitted paraboloid surfaces on detected local maxima. S_i represents a cluster with two true tree tops; S_j shows a false positive cluster with at least one wrongly detected local maximum.

$$E = \begin{bmatrix} a & h & g & p \\ h & b & f & q \\ g & f & c & r \\ p & q & r & d \end{bmatrix} \tag{3}$$

where E stands for the coefficient matrix of the surface. The quadratic surfaces have different standard form types. In this study, we use the elliptic paraboloid, a quadratic surface which has an elliptical cross section (Dai et al., 2007). We assume the paraboloid axis is known and coincides with the world Z axis due to the phenomenon of gravitropism of trees. Therefore, the simplified version of the Eq. (2) as an elliptic paraboloid of height z_c, semi-major axis a and semi-minor axis b without any rotation angle can be specified parametrically as a function of (x,y):

$$Z(x,y) = -\frac{(x-x_c)^2}{a^2} - \frac{(y-y_c)^2}{b^2} + z_c \tag{4}$$

The paraboloid's center (x_c,y_c,z_c) is fixed to the current detected local maximum, whereas the semi-axis lengths, a and b, need to be determined through RANSAC estimation.

3.3.2. Details of RANSAC estimation

Consider two samples (x_0,y_0,z_0) and $(x_1,y_1;z_1)$ with (x_c,y_c,z_c) as the fixed center of the paraboloid. It is possible to calculate the axis lengths a and b for the aforementioned samples, by using the following equation (Eq. (5)).

$$\begin{bmatrix} (x_0-x_c)^2 & (y_0-y_c)^2 \\ (x_1-x_c)^2 & (y_1-y_c)^2 \end{bmatrix} \begin{bmatrix} 1/a^2 \\ 1/b^2 \end{bmatrix} = \begin{bmatrix} z_0-z_c \\ z_1-z_c \end{bmatrix} \tag{5}$$

After calculating the axis lengths a and b for all points, their distances to the paraboloid surface are determined. Additionally, the absolute distance $|z-z_i|$ is taken as the error measure for the RANSAC.

3.4. Classification

Although the RANSAC procedure yields the optimal paraboloid shape anchored at the chosen local maximum, it is still possible that the paraboloid does not represent a true, distinct tree top, but rather is located to the side of an adjacent, dominant tree (see Fig. 3). Therefore, it is necessary to further classify each fitted paraboloid based on its spatial characteristics in order to retain only those representing true tree tops. We use a kernelized logistic regression (KLR) with L_2 norm regularization as a classifier. Logistic regression models the probability distribution of the class label Y and histograms X (see Section 3.4.1) as follows:

$$P(Y=1|X=x) = \frac{1}{1+\exp\left[-\sum_{j=1}^{N} \alpha_j k(x_i,X)\right]} \tag{6}$$

where $j,j = 1...N$ denotes N feature vectors of training examples and Y the corresponding binary label. The term k represents a positive semi-definite kernel function. Training the model amounts to maximizing the regularized log-likelihood of the training examples in Eq. (6) as:

$$\max_{\alpha} \ell(\alpha) - \frac{\lambda}{2}\alpha^T K\alpha \tag{7}$$

where $K = (k(x_i,x_j))_{1,\dots,N,1,\dots,N}$ represents the design matrix, and the expression $\alpha^T K\alpha$ denotes the L_2 norm regularization term. Eq. (7) represents a convex optimization problem that was solved by the Newton-Raphson method (Roscher et al., 2012). The model's log-likelihood and the functional form of the used Gaussian kernel are given respectively by Eqs. (8) and (9).

$$\ell(\alpha) = \sum_{j=1}^{N} \log P(Y=y_i|X=x_i) \tag{8}$$

$$K_\gamma(x_i,y_j) = \exp\left(-\frac{1}{2}\frac{|x_i-x_j|^2}{\gamma}\right) \tag{9}$$

where x_i and x_j are two sample feature vectors. The two main parameters, Gaussian kernel bandwidth γ and regularization coefficient λ, are determined by a grid search on an exponential grid, using Cohen's kappa coefficient as the error measure and 10-fold cross-validation. We classify the candidate local maxima (and their associated paraboloids) of single coniferous trees into two classes: "positive" and "negative", respectively. The "positive" class corresponds to true tree tops, whereas the "negative" class indicates false positives. See Section 4.2 for a description of the training procedure.

3.4.1. Elliptic paraboloids features

The features for classifying the local maxima are based on projected distances of local points to the fitted shape. Specifically, we consider all points located in the aforementioned cylinder around the local maximum (see Section 3.3) and compute an approximate projection onto the paraboloid using the algebraic distance, i.e. for a point $Q_i = (x_i,y_i,z_i)$ we take the point $(x_i,y_i,Z(x_i,y_i))$, where $Z(x_i,y_i)$ is the fitted surface's Z position at coordinate (x,y), as in Eq. (4). We decided to use this approximate method instead of a true projection onto the paraboloid due to the fact that computing the true projection of a point onto a quadric requires solving a 6-th degree polynomial equation for each point (Dai et al., 2007), which could be prohibitively computationally expensive. The signed distance from point Q_i to the surface is thus $z_i - Z(x_i,y_i)$. In this part of our method, the signed distances are binned to form histogram features, X, for the classification purpose mentioned in the Section 3.4. These features capture the shape of the point distributions around the apices of the paraboloids. Fig. 4 shows the process of generating features for the classification of local maxima. For local maxima representing true tree tops, the distances should be approximately symmetrically distributed around zero, while for the case of a false local maximum depicted in Fig. 3 (S_j), the signed distance distribution should be significantly biased towards large positive residuals.

3.5. Calculating spatial overlap ratio

After the classification step, a number of fitted paraboloids remain which represent the detected true tree tops. However, in some cases more than one local maximum may represent the same tree, which

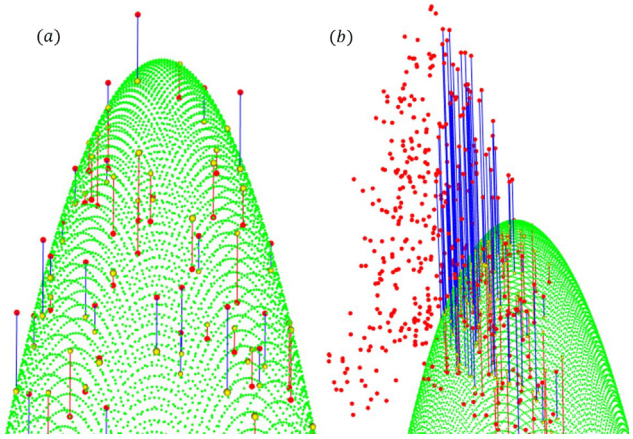

Fig. 4. Signed distances between data points (in red) and their approximate projections (in yellow) onto the fitted paraboloid (green). Positive and negative distances are indicated respectively by blue and red lines. (a) Residuals around a true tree top, distributed symmetrically around zero, (b) Residuals around a false local maximum located at the side of the tree, showing bias towards large positive values. (For interpretation of the references to colour in this figure legend, the reader is referred to the web version of this article.)

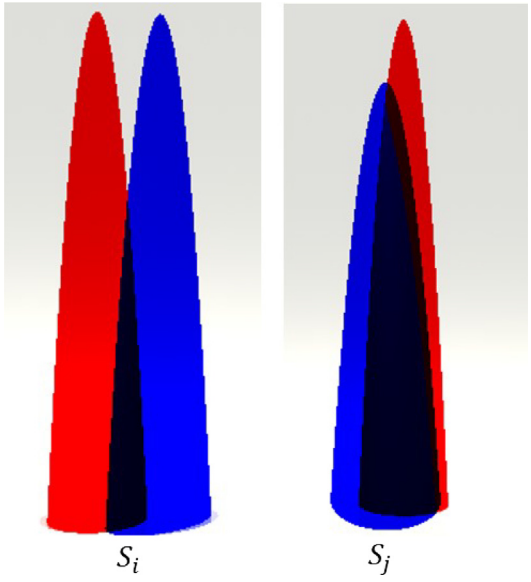

Fig. 5. Estimating the spatial overlap ratio op_r between fitted paraboloid surfaces. S_i represents a cluster with 2 true tree tops; S_j shows a false positive cluster with at least one falsely detected local maximum.

makes it necessary to filter redundant values. Therefore, we define a feature for a pair of paraboloids S_i and S_j, which evaluates the ratio of their spatial overlap op_r, i.e. the ratio of the volume shared by both shapes to the volume of an individual paraboloid. The ratio is normalized between a value of zero and one, corresponding to no overlap and full overlap between the paraboloids, respectively. If the overlap ratio exceeds the maximum threshold value max_{op_r}, then we assume that both paraboloids represent the same tree. In the current step, since it is difficult to analytically derive parameters for elliptic surfaces, we apply Monte Carlo simulation to estimate the spatial overlap of the fitted paraboloids. Fig. 5 demonstrates the idea behind calculating the intersection volume using a random simulation method. We generate a number of sample points N within the interior of the first paraboloid. Afterwards, for each point, we check the possibility that the point also lies in the second paraboloid. The overlap ratio, op_r, can be approximated as the number of points that are located inside both paraboloids

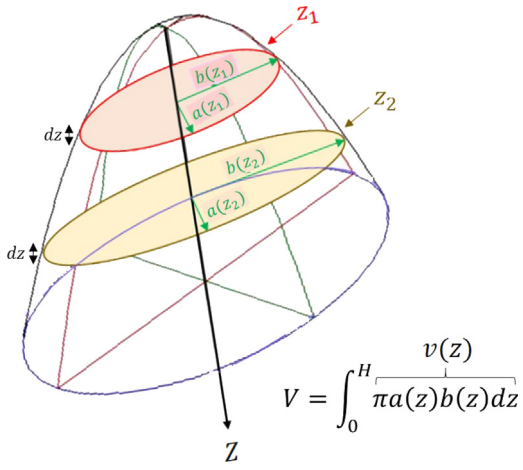

Fig. 6. The entire volume of a paraboloid, V, can be decomposed into an infinite number of elliptical slices with infinitely small thicknesses, dz, and volumes, $v(z)$, which are functions of their heights z. H represents the height of the paraboloid. The number of points generated in each slice should be proportional to its cross-sectional area.

divided by the number of generated sample points, N. Note that in the current experiment, a uniform spatial distribution of the points is generated in the entire volume of the paraboloid. To ensure this uniformity, we perform the sampling in two steps. In the first step, we draw the vertical distance, Z, from the paraboloid center randomly according to the triangular distribution, $P(Z \leqslant z) \propto z^2$. For the second step, we generate a point from the interior of the ellipse that constitutes the cross section of the paraboloid at the drawn height of z from the previous step. Fig. 6 shows the process of uniformly sampling points in the paraboloid. In order to maintain a uniform point density across the entire paraboloid, the local densities in every vertical 'slice' of the volume should be equal. However, the volume of a slice at height z is proportional to z. Since the density remains constant, the number of generated points for a layer must also be proportional to its height. The spatial overlap ratio of paraboloids, op_r, for the adaptive stopping criterion method is given by algorithm Alg. 1. The *rnd*() function in the algorithm refers to the uniform random number generator in the range 0–1. This Monte Carlo based procedure yields an unbiased estimator of the true ratio of overlapping volume.

Algorithm 1. Spatial overlap ratio.

function CalculateSpatialOverlap*para1, para2, N*
  for $l = 1,...,N$ **do**
    $z \leftarrow para1.\ Height\sqrt{rnd()}$
    $\theta \leftarrow 2\pi rnd()$
    $r \leftarrow para1.\ A\sqrt{z}\cdot r\cdot cos(\theta)$
    $x = para2.\ B\sqrt{z}\cdot r\cdot sin(\theta)$
    $y = \sqrt{rnd()}$
    if *para2 contains* (x,y,z) **then**
      $nBoth \leftarrow nBoth + 1$
  return $nBoth/N$

4. Experiment

4.1. Materials

Our experiments were conducted for three sample plots in the Bavarian Forest National Park (49°3′19″N, 13°12′9″E), a temperate forest located in the southeastern part of Germany, along the border with the Czech Republic. The sample plots contain a mixture of mountainous

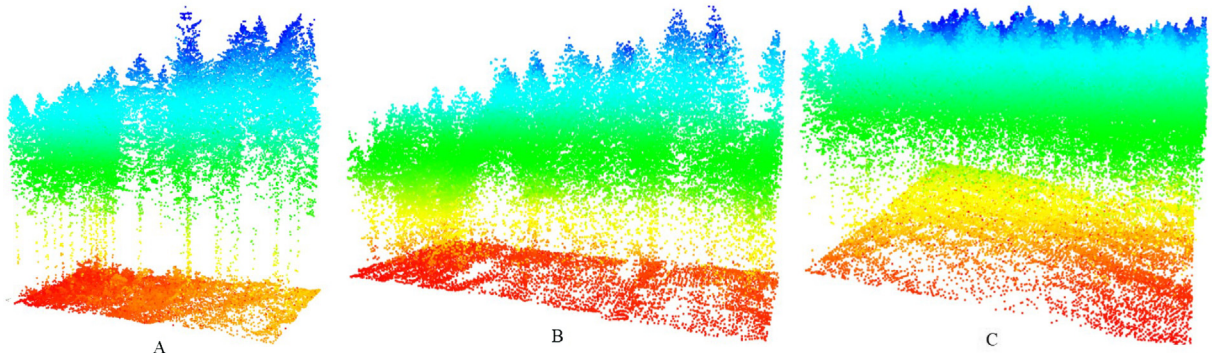

Fig. 7. ALS point clouds of Plot A (100% coniferous), Plot B (99% coniferous) and Plot C (70% coniferous) colored by height over DTM. (For interpretation of the references to colour in this figure legend, the reader is referred to the web version of this article.)

Table 1
Properties of sample plots.

Property	Plot A	Plot B	Plot C
Size [ha]	0.10	0.10	0.30
Trees/ha	450	2150	700
Ave. DBH[a] (cm)	46.2	17.9	35.0
Ave. Crown base height (m)	20.90	7.08	16.70
Ave. Tree height (m)	36.90	16.08	35.45
Dominant species	Spruce	Spruce	Spruce
Deciduous trees[%]	0	1	29
Understory trees [Number]	0	76	11
Intermediate layer [Number]	4	85	33
Overstory trees [Number]	41	54	165

[a] Diameter at Breast Height.

and subalpine forest types, dominated by Norway spruce (*Picea abies*) and European beech (*Fagus sylvatica*) (Cailleret et al., 2014). The airborne full-waveform data were acquired using a Riegl LMS-Q560 scanner in May 2007 in a leaf-on condition with an average point density of 25 points/m^2. The flying altitude of 400 m resulted in a footprint size of 20 cm. We used the mixture-of-Gaussians decomposition model (Reitberger et al., 2009) on the collected waveforms, obtaining a 3D point cloud. The 3D visualization of point clouds for the plots (coniferous-dominated stands) is shown in Fig. 7. Table 1 summarizes the characteristics of our sample plots, estimated based on the reference data from the field inventory.

4.2. Classifier training

Additionally, we chose 100 point cloud clusters from areas outside the test plots as training data for the local maxima classifier. The clusters consisted both of scenes containing only a single tree and ones comprising multiple adjacent trees, in order to ensure a wide range of training scenarios (with the proportion of 50–50%). These clusters were obtained from various intermediate steps, i.e. partial segmentations, of the standard normalized cut algorithm with the static normalized cut threshold $NCut_{thr}$. For each training cluster, the local maxima detection was performed, and each local maximum was labeled as either a true tree top or a false positive, based on visual interpretation of the point cloud. The paraboloid-based features (see Section 3.4.1) were extracted for each local maximum. The set of all extracted features together with the local maxima labels formed the basis for training the classifier to detect the characteristic paraboloid shape of coniferous trees. The classifier provides a probability of p that a local maximum represents a "true positive", i.e. tree top. Later, the minimum acceptance probability threshold $min_{p_{thr}}$ is used as a control parameter, i.e. a local maximum is processed further if its probability p exceeds this threshold value.

4.3. Reference data

The ground truth data for the test plots was acquired by field measurements. In each of the 3 plots, at least 40 single trees with DBH greater than 10 cm were present. Several individual tree parameters such as total tree height, stem position, DBH, and tree species were measured with the help of GPS and tacheometry. Moreover, the single trees in the scene are subdivided into three layers with respect to the top tree height h_{top} in the plot. The top tree height h_{top} is defined as the average height of the 100 highest trees per ha (Heurich, 2006). The lower layer contains all trees below 50% of h_{top}, the intermediate layer corresponds to all trees between 50% and 80% of h_{top}, and the upper layer refers the remainder of the trees. Plot A has no trees at the understory layer and fewer than 10% of total number of trees at the intermediate layer. However, plot B contains a higher number of trees at intermediate and understory layers compared to plots A and C. Plot B has the highest number of trees at the intermediate and understory layers among the other plots. In this study, we removed both lower and intermediate layers based on the top tree height h_{top} and focused on the upper layer, where the single tree crowns are clearly shaped as elliptic paraboloids. There were a total of 260 single trees in the three sample plots.

4.4. Experimental setup

We conducted four groups of experiments. These experiments are concerned with assessing the performance of the entire method for single tree segmentation, particularly the benefit of using the newly introduced adaptive stopping criterion. For the first two sets, we used the basic normalized cut segmentation algorithm with normalized cut threshold $NCut_{thr}$. In the other two groups of experiments, tree segmentation was based on our adaptive stopping criterion. To demonstrate that our approach is independent of the segmentation granularity, we executed the experiments with two kinds of primitives for merging: (i) voxel-based and (ii) those obtained from mean shift clustering. In the voxel-based approach, the concept is to subdivide the tree into a voxel space, which results in equal-sized primitives in the form of voxels with a side length $d_{vox} = 0.5$ m. In contrast, the mean shift algorithm generates a segmentation of the point cloud consisting of non-uniformly sized clusters. We used a cylindrical kernel with base radius $h_r = 2.4$ m and height $H = 2.4$ m (see Yao et al. (2013)). The similarity function was the standard exponential model as in Reitberger et al. (2009). The adjacency relation of the graph was based on a cylindrical neighborhood with a predefined radius and unlimited height, as described in our previous work (Amiri et al., 2016). Aside from geometric information, the similarity function contained a term reflecting the mean pulse intensities and widths averaged over the clusters' member points.

Table 2
Control parameters of the adaptive stopping criterion method for single tree segmentation.

Parameters	Symbols	Values
Maximum overlap ratio	max_{op_r}	0.3
Minimum probability threshold	$min_{P_{thr}}$	0.5
Local maxima neighborhood radius	r_{neig}	1.2
Signed distance bin width	sd_{bw}	1.0
Signed distance range	sd_{range}	20.0
Cylinder length	cyl_l	5.0
Cylinder radius	cyl_r	1.0
RANSAC inlier distance	sac_d	0.05

4.5. Choice of parameters

The different control parameter values that we used in our approach are summarized in the Table 2. The values were assigned empirically based on the forest characteristics. The cylinder radius cyl_r is based on the largest radius of a single coniferous tree crown that we expect to find in the plots. Similarly, the cylinder length cyl_l approximates the maximum expected range of the upper tree crown in the study area. Moreover, the local maxima neighborhood radius r_{neig} corresponds roughly to the average size of the tree crown segments. Consistent parameter values were used for all test plots.

4.6. Evaluation

The output of our processing pipeline consists of a set of points that correspond to the individual segmented trees. The matching between segmented and reference trees was calculated using the strategy proposed by Reitberger et al. (2009). We considered the segmented and reference trees as matched if (i) the distance to the reference single tree is less than 60% of the mean tree distance within the sample plot and (ii) the height difference between and the height of the reference tree is less than 20% of the top height of the plot. Moreover, if a reference tree is associated with more than one tree position, the tree position with the shortest distance to the reference tree is taken. A segmented tree cluster without a link to a reference tree is called a “false positive” segment.

In the current experiment, we use the “correctness” and “completeness” metrics to measure the quality of the obtained segmentation results. The “correctness” metric is defined as the number of segmented trees that were successfully linked to reference trees as a fraction of the total number of segmented trees. The “completeness” expresses the ratio of the number of reference trees that have at least one associated segmented tree to the total number of reference trees.

5. Results and discussion

5.1. Sensitivity analysis

Clearly, the adaptive stopping criterion approach requires proper values for the control parameters. We conducted tests to find the values of the most important parameters and their sensitivity. We demonstrate the performance of the adaptive stopping criterion with two main control parameters: the maximum overlap ratio, max_{op_r}, and minimum probability threshold, $min_{P_{thr}}$. The results from the maximum overlap ratio, max_{op_r}, showed that smaller values produce relatively higher correctness and completeness. A value of 0.3 represents a good trade-off between the correctness and completeness that can successfully split the cluster into adjacent tree crowns. Fig. 8 shows the segmentation performance by ROC curves on the sample plots mentioned in Section 4.2 when different values of maximum overlap ratio, max_{op_r}, are applied. The three plots dominated by coniferous trees share the property that over 70% of trees can be detected correctly, at the threshold of 0.3 of the spatial overlap between clusters. In plot C, which contains almost 30% deciduous trees, the true positive rate on average did not exceed 65% for various threshold values. Among the test datasets, plot A exhibits relatively higher correctness and completeness rates. In Fig. 9, the adaptive segmentation performance for the probability threshold of the same sample plots (see Section 4.2) is presented by ROC curves. For the minimum probability threshold $min_{P_{thr}}$, 0.5 was selected as an optimal trade-off value. A larger minimum probability threshold, $min_{P_{thr}}$, led to more segments, which resulted in an overall higher completeness but lower correctness across the all the sample plots. The sensitivity analysis of our segmentation method for the selected plots was similar if a minimum probability threshold value, $min_{P_{thr}}$, less than 0.3 was selected. Also, for plot A, the ROC curves with different threshold values continue to increase and attain a completeness of 0.75, whereas on the other two plots, a value of 0.65 is not exceeded. The lowest true positive rate with the highest false positive rate is achieved for plot B. Note that the obtained values of 0.3 for the maximum overlap ratio, max_{op_r}, and 0.5 for the minimum probability threshold, $min_{P_{thr}}$, were nearly optimal on all three considered plots. Moreover, for the baseline experiment, we demonstrate the sensitivity analysis for the normalized cut threshold, $NCut_{thr}$, that controls the subdivision of the segments in the procedure. Tests in terms of correctness and completeness for the sample plots mentioned in Section 4.2 showed the best performance was achieved with a $NCut_{thr}$ value of 0.16.

5.2. Adaptive segmentation approach

The results of the segmentation performance on the upper canopy layer with respect to the two sets of merging primitives: (i) voxel-based and (ii) those obtained from mean shift clustering are summarized in Table 3. For all plots, the correctness and completeness terms are estimated. In the current plots, due to the point density and forest characteristics (particularly deciduous trees), up to 30% of the upper layer trees could not be correctly segmented. The task of adaptive single tree segmentation in the mixed deciduous and coniferous plots proved to be even more challenging than it was for the coniferous dominated stands. In upper canopy layer, the reliability of the method is high because the 3D tree structure captured within the point clouds exhibits the full shape of elliptic paraboloids.

The results in terms of correctness and completeness for the adaptive segmentation by using two different primitives are presented. For three plots, an improvement of 6–9% and 7–10%, respectively, for correctness and completeness is achieved, in comparison to the basic normalized cut segmentation with mean shift primitives. Also, the adaptive approach of the normalized cut with voxel-based primitives for the same plots compared to the basic segmentation with voxel-based step performs a gain of 7–8% and 8–10%, respectively, in terms of correctness and completeness. The experiments on the three plots confirm that higher completeness and correctness rates can be achieved for the adaptive normalized cut with voxel-based and mean shift clustering primitives rather than the basic segmentation approaches. In the case of adaptive segmentation by voxel-based primitives, for plot A the good trade-off results between correctness and completeness rate are 0.65 and 0.77, respectively. For plot B, identical correctness and completeness results for both voxel-based and mean shift primitives are achieved. Finally, for plot C, 0.69 for the completeness and 0.76 for the correctness rate are accomplished. For all the plots, when the adaptive segmentation scenario is applied, the correctness and completeness rates are both increased. The average rate of false detected tree segments in the plot A, B and C amount to 0.23, 0.33 and 0.31, respectively. Note that the method is evaluated by the single trees located in the upper canopy layer.

Figs. 10 and 11 show examples of the segmentation results by primitives obtained from mean shift clustering for a part of test plot A. Note that the sample plot contains only coniferous trees. The results indicate that our method was successful in overcoming the over- and

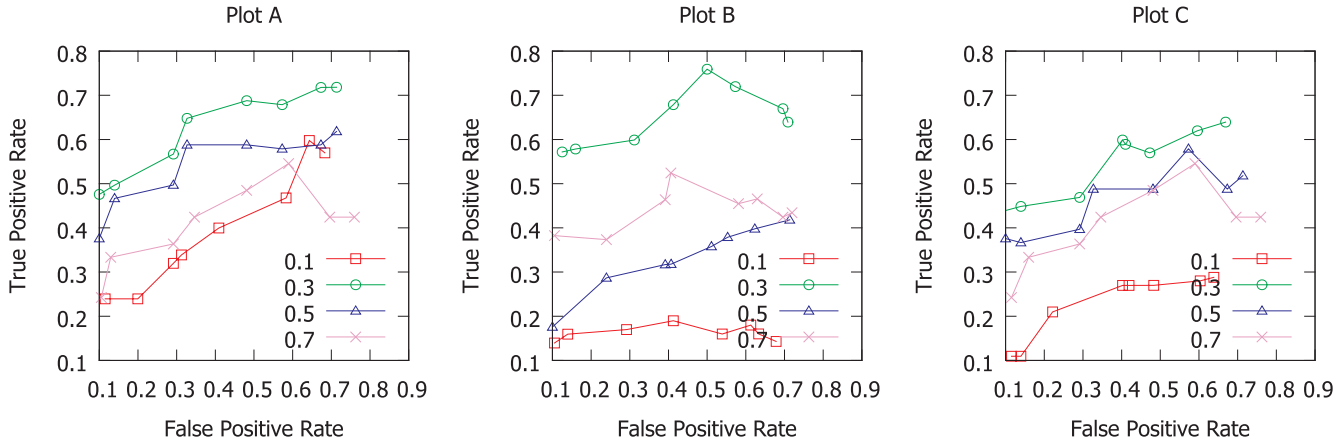

Fig. 8. ROC curve of single tree adaptive segmentation for plots A (100% coniferous), B (99% coniferous) and C (70% coniferous). Each diagram contains four ROC curves that correspond to various thresholds of the maximum overlap ratio, max_{op_r}.

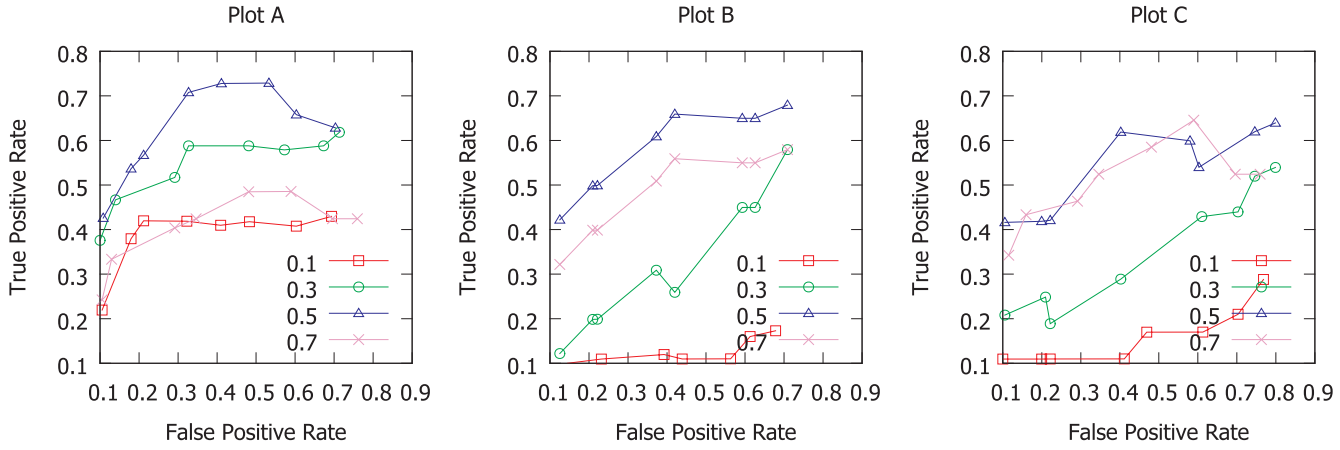

Fig. 9. ROC curve of single tree adaptive segmentation for plots A (100% coniferous), B (99% coniferous) and C (70% coniferous). Each diagram contains four ROC curves that correspond to various thresholds of the minimum probability threshold, $min_{p_{thr}}$.

Table 3
Results of analysis on the upper canopy layer for sample plots A, B, and C.

Segmentation scenario	Plot A	Plot B	Plot C
Completeness			
Mean Shift + NCut	0.69	0.56	0.61
Voxel-based + NCut	0.66	0.58	0.61
Mean Shift + NCut (Adaptive)	0.76	0.67	0.68
Voxel-based + NCut (Adaptive)	0.77	0.67	0.69
Correctness			
Mean shift + NCut	0.59	0.64	0.70
Voxel-based + NCut	0.53	0.63	0.69
Mean shift + NCut (Adaptive)	0.68	0.70	0.79
Voxel-based + NCut (Adaptive)	0.65	0.70	0.76

under-segmentation problems in the test plot. Fig. 10 presents the comparison of segmentation results between the normalized cut combined with mean shift clustering and the adaptive stopping criterion method. The tree clusters are classified using fitted elliptic paraboloids and the spatial overlap ratios between them are calculated. The red box in Fig. 10a shows an over-segmented cluster that is delineated as a single tree (see Fig. 10b) by using the adaptive segmentation approach.

In contrast, the case of under-segmentation is indicated by Fig. 11. In this case, we used the adaptive stopping criterion method to reduce the under-segmentation error of the normalized cut algorithm with clusters obtained from the mean shift step. In Fig. 11a, the red box is focused on an example cluster consisting of multiple trees, which is known as under-segmentation. Using the adaptive segmentation method, it is revealed in Fig. 11b how the under-segmentation for the current cluster is removed.

The computational costs for both the static and adaptive versions were similar, which indicates that the processing time was dominated by solving the generalized eigenvalue problem on the *Ncut* similarity matrix. A simple heuristic may be used to reduce the number of times the adaptive stopping criterion is invoked; for a given point cluster, if its 3D bounding box exceeds the dimensions of the largest possible single object (i.e. tree), the segmentation must continue. In principle our approach is applicable for larger forest areas.

Our method takes the advantage of fitting elliptic paraboloids to point clouds and determining whether the currently processed cluster of points represents a single coniferous tree or multiple trees. The sensitivity analysis shows that for all the sample plots the same set of parameters, such as maximum overlap ratio, max_{op_r}, and minimum probability threshold, $min_{p_{thr}}$, achieves the best trade-off values between correctness and completeness. The restrictions of the current approach are: (i) mainly trees in the upper canopy layer in the 3D point cloud can be segmented accurately, (ii) the method fails in plots with concentrations of deciduous trees where the segments' points cannot be clearly clustered. The crown boundaries of deciduous trees are not clear in the point clouds due to the complex geometry of these trees in the leaf-on condition. Therefore, no benefit was achieved, despite the adaptive segmentation approach, for deciduous trees. In the case where the study area is dominated by coniferous trees, single tree segments are successfully delineated by the classifier training and elliptic

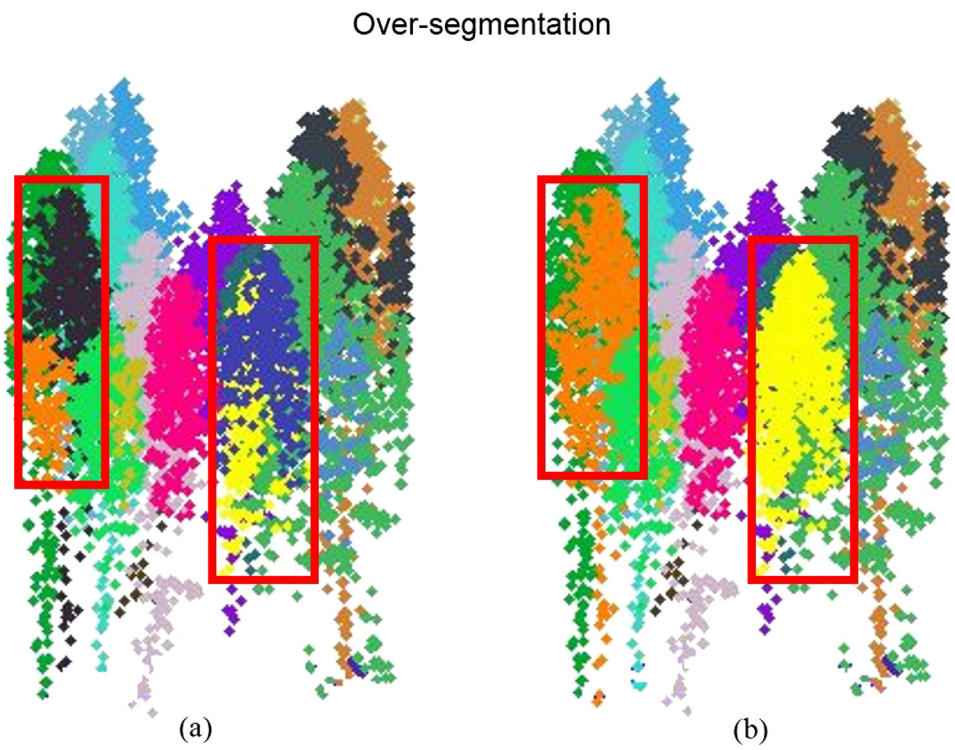

Fig. 10. Single tree segmentation results for a part of plot A: (a) corresponds to the normalized cut segmentation with mean shift clustering results; and (b) represents the adaptive stopping criterion for normalized cut segmentation by fitting paraboloids. Each set of colored points represents a delineated single tree. The red boxes outline the over-segmentation issue on an example single tree. (For interpretation of the references to colour in this figure legend, the reader is referred to the web version of this article.)

paraboloids fitting method. Moreover, the normalized cut threshold $NCut_{thr}$ has no physical meaning; however, our method's main control parameters are closely tied with the appearance of single trees in the forest scene, which makes them more easily interpretable.

6. Conclusions

The study presents a novel method for single tree segmentation in temperate coniferous forest by applying an adaptive stopping criterion to top-down segmentation in ALS point clouds. Following the study on segmentation of fallen stems (Polewski et al., 2015), our results also confirm that the use of an appearance-based stopping criterion can benefit a top-down segmentation process in different scenarios. Our method is directly applied to the 3D ALS point clouds, targeting coniferous trees through modeling their crowns by elliptic paraboloids. The adaptive segmentation approach generally appears to lead to an improvement of up to 10% in both correctness and completeness. We did not try to include the tree species composition in the analysis; this will constitute a topic of future research. Moreover, the accuracy of the segmentation was negatively impacted by the higher number of deciduous trees in the upper canopy layer. Further improvements to the method would be achieved by extending the adaptive segmentation approach to the deciduous tree species to deal with the over- and under-segmentation problems. Although some deciduous tree species may follow a well-defined geometric crown shape, it is challenging to propose a single model that can accurately represent all broad-leaf trees. However, higher point density ALS data, as well as data acquisition in leaf-off condition, could lead to more precise reconstruction of the single tree segments. Furthermore, we would like to utilize the stems obtained from the method proposed by Amiri et al. (2017) to enhance the single tree segmentation in the intermediate and lower canopy layers by providing prior knowledge about tree locations.

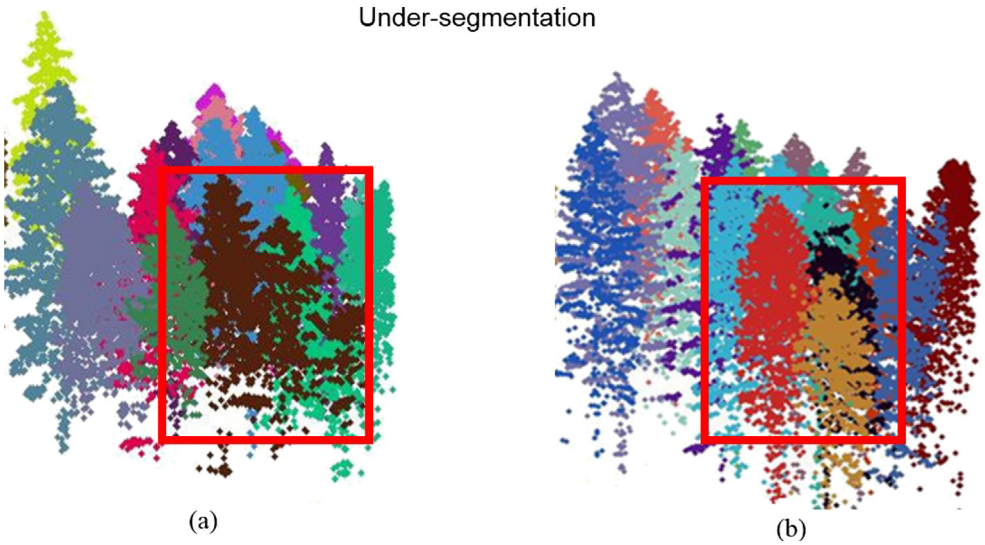

Fig. 11. Single tree segmentation results for a part of plot A: (a) corresponds to the normalized cut segmentation with mean shift clustering results; and (b) represents the adaptive stopping criterion for the normalized cut segmentation by fitting paraboloids. Each set of colored points shows a delineated single tree. The red boxes outline the under-segmentation issue on an example group of single trees. (For interpretation of the references to colour in this figure legend, the reader is referred to the web version of this article.)

References

Amiri, N., Polewski, P., Yao, W., Krzystek, P., Skidmore, A., 2017. Detection of single tree stems in forested areas from high density als point clouds using 3d shape descriptors. ISPRS Annals Photogram., Remote Sens. Spatial Inform. Sci. 35–42.

Amiri, N., Yao, W., Heurich, M., Krzystek, P., Skidmore, A.K., 2016. Estimation of regeneration coverage in a temperate forest by 3d segmentation using airborne laser scanning data. Int. J. Appl. Earth Obs. Geoinf. 52, 252–262.

Cailleret, M., Heurich, M., Bugmann, H., 2014. Reduction in browsing intensity may not compensate climate change effects on tree species composition in the bavarian forest national park. For. Ecol. Manage. 328, 179–192.

Chang, A., Eo, Y., Kim, Y., Kim, Y., 2013. Identification of individual tree crowns from lidar data using a circle fitting algorithm with local maxima and minima filtering. Remote Sens. Lett. 4 (1), 29–37.

Dai, M., Newman, T.S., Cao, C., 2007. Least-squares-based fitting of paraboloids. Pattern Recogn. 40 (2), 504–515.

Fischler, M.A., Bolles, R.C., 1981. Random sample consensus: a paradigm for model fitting with applications to image analysis and automated cartography. Commun. ACM 24 (6), 381–395.

González-Ferreiro, E., Diéguez-Aranda, U., Barreiro-Fernández, L., Buján, S., Barbosa, M., Suárez, J.C., Bye, I.J., Miranda, D., 2013. A mixed pixel-and region-based approach for using airborne laser scanning data for individual tree crown delineation in pinus radiata d. don plantations. Int. J. Remote Sens. 34 (21), 7671–7690.

Heurich, M., 2006. Evaluierung und Entwicklung von Methoden zur automatisierten Erfassung von Waldstrukturen aus Daten flugzeuggetragener Fernerkundungssensoren (Ph.D. thesis). Technische Universität München.

Heurich, M., 2008. Automatic recognition and measurement of single trees based on data from airborne laser scanning over the richly structured natural forests of the bavarian forest national park. For. Ecol. Manage. 255 (7), 2416–2433.

Hu, B., Li, J., Jing, L., Judah, A., 2014. Improving the efficiency and accuracy of individual tree crown delineation from high-density lidar data. Int. J. Appl. Earth Obs. Geoinf. 26, 145–155.

Husch, B., Beers, T., Kershaw, J., 2002. Forest Mensuration. Ecology (John Wiley and Sons). John Wiley & Sons. <https://books.google.de/books?id=p0v3m8Pau-kC>.

Hyyppä, J., Kelle, O., Lehikoinen, M., Inkinen, M., 2001. A segmentation-based method to retrieve stem volume estimates from 3-d tree height models produced by laser scanners. IEEE Trans. Geosci. Remote Sens. 39 (5), 969–975.

Khosravipour, A., Skidmore, A.K., Isenburg, M., Wang, T., Hussin, Y.A., 2014. Generating pit-free canopy height models from airborne lidar. Photogramm. Eng. Remote Sens. 80 (9), 863–872.

Koop, H., 1989. Forest Dynamics: SILVI-STAR, a Comprehensive Monitoring System. Springer-Verlag.

Lee, H., Slatton, K.C., Roth, B., Cropper Jr, W., 2010. Adaptive clustering of airborne lidar data to segment individual tree crowns in managed pine forests. Int. J. Remote Sens. 31 (1), 117–139.

Li, W., Guo, Q., Jakubowski, M.K., Kelly, M., 2012. A new method for segmenting individual trees from the lidar point cloud. Photogramm. Eng. Remote Sens. 78 (1), 75–84.

Morsdorf, F., Meier, E., Kötz, B., Itten, K.I., Dobbertin, M., Allgöwer, B., 2004. Lidar-based geometric reconstruction of boreal type forest stands at single tree level for forest and wildland fire management. Remote Sens. Environ. 92 (3), 353–362.

Nie, F., Ding, C., Luo, D., Huang, H., 2010. Improved minmax cut graph clustering with nonnegative relaxation. In: Joint European Conference on Machine Learning and Knowledge Discovery in Databases. Springer, pp. 451–466.

Persson, A., Holmgren, J., Söderman, U., 2002. Detecting and measuring individual trees using an airborne laser scanner. Photogramm. Eng. Remote Sens. 68 (9), 925–932.

Polewski, P., Yao, W., Heurich, M., Krzystek, P., Stilla, U., 2015. Detection of fallen trees in als point clouds using a normalized cut approach trained by simulation. ISPRS J. Photogramm. Remote Sens. 105, 252–271.

Pyysalo, U., Hyyppä, H., 2002. Reconstructing tree crowns from laser scanner data for feature extraction. Int. Arch. Photogram. Remote Sens. Spatial Inform. Sci. 34 (3/B), 218–221.

Reitberger, J., Schnörr, C., Krzystek, P., Stilla, U., 2009. 3d segmentation of single trees exploiting full waveform lidar data. ISPRS J. Photogram. Remote Sens. 64 (6), 561–574.

Roscher, R., Förstner, W., Waske, B., 2012. I 2 vm: incremental import vector machines. Image Vis. Comput. 30 (4), 263–278.

Savaresi, S.M., Boley, D.L., 2001. On the performance of bisecting k-means and pddp. In: Proceedings of the 2001 SIAM International Conference on Data Mining. SIAM, pp. 1–14.

Shi, J., Malik, J., 2000. Normalized cuts and image segmentation. IEEE Trans. Pattern Anal. Mach. Intell. 22 (8), 888–905.

Solberg, S., Naesset, E., Bollandsas, O.M., 2006. Single tree segmentation using airborne laser scanner data in a structurally heterogeneous spruce forest. Photogramm. Eng. Remote Sens. 72 (12), 1369–1378.

Strîmbu, V.F., Strîmbu, B.M., 2015. A graph-based segmentation algorithm for tree crown extraction using airborne lidar data. ISPRS J. Photogram. Remote Sens. 104, 30–43.

Vauhkonen, J., Ene, L., Gupta, S., Heinzel, J., Holmgren, J., Pitkänen, J., Solberg, S., Wang, Y., Weinacker, H., Hauglin, K.M., et al., 2011. Comparative testing of single-tree detection algorithms under different types of forest. Forestry 85 (1), 27–40.

Véga, C., Hamrouni, A., El Mokhtari, S., Morel, J., Bock, J., Renaud, J.-P., Bouvier, M., Durrieu, S., 2014. Ptrees: a point-based approach to forest tree extraction from lidar data. Int. J. Appl. Earth Obs. Geoinf. 33, 98–108.

Wagner, W., Hollaus, M., Briese, C., Ducic, V., 2008. 3d vegetation mapping using small-footprint full-waveform airborne laser scanners. Int. J. Remote Sens. 29 (5), 1433–1452.

Wang, Y., Weinacker, H., Koch, B., 2008. A lidar point cloud based procedure for vertical canopy structure analysis and 3d single tree modelling in forest. Sensors 8 (6), 3938–3951.

Wu, B., Yu, B., Wu, Q., Huang, Y., Chen, Z., Wu, J., 2016. Individual tree crown delineation using localized contour tree method and airborne lidar data in coniferous forests. Int. J. Appl. Earth Obs. Geoinf. 52, 82–94.

Wu, Z., Leahy, R., 1993. An optimal graph theoretic approach to data clustering: theory and its application to image segmentation. IEEE Trans. Pattern Anal. Mach. Intell. 15 (11), 1101–1113.

Wulder, M.A., White, J.C., Nelson, R.F., Næsset, E., Ørka, H.O., Coops, N.C., Hilker, T., Bater, C.W., Gobakken, T., 2012. Lidar sampling for large-area forest characterization: a review. Remote Sens. Environ. 121, 196–209.

Yao, W., Krull, J., Krzystek, P., Heurich, M., 2014. Sensitivity analysis of 3d individual tree detection from lidar point clouds of temperate forests. Forests 5 (6), 1122–1142.

Yao, W., Krzystek, P., Heurich, M., 2012. Tree species classification and estimation of stem volume and dbh based on single tree extraction by exploiting airborne full-waveform lidar data. Remote Sens. Environ. 123, 368–380.

Yao, W., Krzystek, P., Heurich, M., 2013. Enhanced detection of 3d individual trees in forested areas using airborne full-waveform lidar data by combining normalized cuts with spatial density clustering. ISPRS Annals Photogram., Remote Sens. Spatial Inform. Sci. 1, 349–354.

Yu, X., Hyypp, J., Vastaranta, M., Holopainen, M., Viitala, R., 2011. Predicting individual tree attributes from airborne laser point clouds based on the random forests technique. ISPRS J. Photogram. Remote Sens. 66 (1), 28–37.

Zhang, K., Chen, S.-C., Whitman, D., Shyu, M.-L., Yan, J., Zhang, C., 2003. A progressive morphological filter for removing nonground measurements from airborne lidar data. IEEE Trans. Geosci. Remote Sens. 41 (4), 872–882.